



Emergence of linear isotropic elasticity in amorphous and polycrystalline materialsShivam Mahajan,¹ Joyjit Chattoraj^{1,2} , and Massimo Pica Ciamarra^{1,3,*} ¹*Division of Physics and Applied Physics, School of Physical and Mathematical Sciences, Nanyang Technological University, Singapore 637371, Singapore*²*Institute of High Performance Computing, Agency for Science, Technology and Research, Singapore 138632, Singapore*³*CNR-SPIN, Dipartimento di Scienze Fisiche, Università di Napoli Federico II, I-80126, Napoli, Italy*

(Received 10 February 2021; accepted 22 April 2021; published 10 May 2021)

We investigate the emergence of isotropic linear elasticity in amorphous and polycrystalline solids via extensive numerical simulations. We show that the elastic properties are correlated over a finite length scale ξ_E , so that the central limit theorem dictates the emergence of continuum linear isotropic elasticity on increasing the specimen size. The stiffness matrix of systems of finite size $L > \xi_E$ is obtained, adding to that predicted by linear isotropic elasticity a random one of spectral norm $(L/\xi_E)^{-3/2}$ in three spatial dimensions. We further demonstrate that the elastic length scale corresponds to that of structural correlations, which in polycrystals reflect the typical size of the grain boundaries and length scales characterizing correlations in the stress field. We finally demonstrate that the elastic length scale affects the decay of the anisotropic long-range correlations of locally defined shear modulus and shear stress.

DOI: [10.1103/PhysRevE.103.052606](https://doi.org/10.1103/PhysRevE.103.052606)**I. INTRODUCTION**

Linear isotropic elasticity (LIE) describes the mechanical response of macroscopic molecular solids, assuming matter is continuous and rotationally invariant. These assumptions are not met at the microscopic scale. Indeed, the elastic properties of small polycrystalline [1] or amorphous [2] samples exhibit large sample-to-sample fluctuations. Similar size fluctuations characterize the elastic response in the plastic regime, where they have been extensively investigated (see, e.g., [3]). The elastic response fluctuations vanish as the linear size of a sample increases and LIE becomes more accurate. Accordingly, LIE's validity depends on the ratio between the linear system size L and a microscopic elastic length scale ξ_E . What sets this length scale? And how does the validity of LIE depend on L/ξ_E ? These questions have been separately addressed in amorphous and polycrystalline materials.

For amorphous solids, extensive simulations have investigated the convergence of the elastic response to linear isotropic elasticity in model Lennard-Jones-like systems. Tanguy *et al.* [4] found the stress anisotropy to decrease exponentially with the system size with a decay length of the order of 65 particle diameters, which is a possible estimation of ξ_E . This length scale has been associated with the correlation length of the nonaffine particle displacements induced by external deformations, which is also, typically, of the order of several diameters [2,4,5]. Subsequent work [6] showed that the eigenvalues of the stiffness tensor evaluated over a coarse-graining length scale w converge to their asymptotic limit as a power law not complying with the central limit theorem expectation and possibly dependent on the degree of structural order [7]. We note, however, that these results

may depend on the chosen definition of coarse-grained elastic quantities [8].

For polycrystals, the question of how the validity of LIE depends on ξ_E/L has not been addressed. Previous works, indeed, mostly investigated how the elastic properties relate to those of the single grains in the limit $L/\xi_E \gg 1$, e.g., through the Voigt [9] or Reuss [10] averages or more refined approaches [11,12]. In polycrystals, the length scale ξ_E is heuristically identified with the typical grain size [13], despite concerns about the connection between structural and elastic length scales [14].

In this paper, we investigate the emergence of LIE in materials with different degrees of structural disorder, from amorphous to polycrystalline, produced via large-scale three-dimensional numerical simulations of the cooling process of liquid samples at different cooling rates (Sec. II). We demonstrate in Sec. III that deviations from LIE scale with the linear size L of the system as $(L/\xi_E)^{-3/2}$, where ξ_E is an elastic correlation length. This result implies that finite-size effects act as a random perturbation to the stiffness matrix, as we discuss in Sec. IV. We further show in Sec. V that the correlation length ξ_E , which grows as the cooling rate decreases, (i) corresponds to a structural correlation length ξ_S which for polycrystalline materials coincides with the grain size and (ii) controls the size dependence of the pressure and anisotropy of the stress tensor. Finally, in Sec. VI we study the correlation of locally defined stress and compliance tensors. We show that these tensors are characterized by long-range anisotropic correlations, confirming previous findings [15–18], and show that the decay of these correlations is governed by the elastic length scale ξ_E .

II. NUMERICAL MODEL AND PROTOCOLS

We perform large-scale numerical simulations of monodisperse spherical particles of diameter σ interacting via the

*massimo@ntu.edu.sg

Hertzian potential, $v(r) = \frac{2}{5}\epsilon(r - \sigma)^{5/2}$ for $r < \sigma$ and $v(r) = 0$ otherwise. We fix the volume fraction to $\phi = 0.74$, a value at which the ground state is an fcc crystal [19], and prepare solid samples by quenching equilibrated liquid configurations to low temperature, using periodic boundary conditions. We mimic quenches to temperatures well below the melting one T_m by first cooling the system to $T_l \simeq 0.8T_m$ at rate Γ and then minimizing the energy via the conjugate-gradient algorithm. The cooling rate affects the ordering properties of the

resulting configuration, which is amorphous at large Γ and polycrystalline at small Γ , which is apparent from Fig. 1. For each cooling rate Γ and number of particles N , in the range of 500 to 1 million, we prepare 50 independent samples. All data reported in the following are averaged over these samples.

III. EMERGENCE OF LINEAR ISOTROPIC ELASTICITY

According to LIE, in three dimensions, the stress-strain relation $\hat{\sigma} = \hat{\mathbf{C}}\hat{\epsilon}$ is

$$\begin{pmatrix} \sigma_1 \\ \sigma_2 \\ \sigma_3 \\ \sigma_4 \\ \sigma_5 \\ \sigma_6 \end{pmatrix} = \begin{pmatrix} \lambda + 2\mu & \lambda & \lambda & 0 & 0 & 0 \\ \lambda & \lambda + 2\lambda & \lambda & 0 & 0 & 0 \\ \lambda & \lambda & \lambda + 2\mu & 0 & 0 & 0 \\ 0 & 0 & 0 & 2\mu & 0 & 0 \\ 0 & 0 & 0 & 0 & 2\mu & 0 \\ 0 & 0 & 0 & 0 & 0 & 2\mu \end{pmatrix} \begin{pmatrix} \epsilon_1 \\ \epsilon_2 \\ \epsilon_3 \\ \epsilon_4 \\ \epsilon_5 \\ \epsilon_6 \end{pmatrix}. \quad (1)$$

Here, suffixes 1–6 indicate xx, yy, zz, xy, xz, yz so that, e.g., c_{14} stands for c_{xxyy} . The parameters $\lambda = \frac{\nu E}{(1+\nu)(1-2\nu)}$ and $\mu = G = \frac{E}{2(1+\nu)}$ are the Lamé constants, and E , G , and ν are Young's modulus, the shear modulus, and Poisson's ratio, respectively. If LIE holds, the six invariants of the stress tensor $\hat{\mathbf{C}}$ are 2μ , with multiplicity of 5, and $3\lambda + 2\mu$, with single multiplicity. However, in finite systems rotational invariance is broken, and hence, $\hat{\mathbf{C}}$ is a symmetric matrix with entries depending on the reference frame. A frame-independent evaluation of the LIE's validity [6] is thus obtained by comparing the invariants of $\hat{\mathbf{C}}$ with those predicted by LIE.

To evaluate the stiffness matrix, we impose on each configuration a strain deformation followed by energy minimization. We perform this operation for the six deformation modes $d(\epsilon_{\alpha\beta})$. In the linear response regime, which we have checked occurs for strains $d(\epsilon_{\alpha\beta}) \lesssim 10^{-7}$, this allows evaluating the stiffness matrix $c_{\alpha\beta\gamma\delta}$ from the changes in the stress tensor $d(\sigma_{\alpha\beta})$,

$$c_{\alpha\beta\gamma\delta}(N) = \frac{d(\sigma_{\alpha\beta})}{d(\epsilon_{\gamma\delta})}. \quad (2)$$

The subsequent diagonalization of the stiffness matrix yields six eigenvalues, which we indicate by $c_1 \leq \dots \leq c_5 \leq b$.

We observe the sample average of the largest eigenvalue $\langle b \rangle$ becomes asymptotically size independent, $\langle b \rangle - (3\lambda + 2\mu) \propto N^{-k_b}$, with $k_b \simeq 0$, as illustrated in Fig. 2(a). $\langle b \rangle$ decreases with Γ , a finding explained considering that, at constant volume, ordered systems have a smaller pressure, as in Fig. 1. When the effect of pressure is filtered out by investigating $\langle b \rangle / \langle P \rangle$, ordered systems are stiffer than disordered ones. At each Γ , the five eigenvalues $\langle c_i \rangle$ approach a common limiting value 2μ as the system size increases. We find, in particular, that c_1 and c_2 approach the asymptotic value from below and c_4 and c_5 approach it from above, while $c_3 \simeq 2\mu$ regardless of the system size. As an example, we illustrate the size dependence of the eigenvalues in Fig. 2(b) for $\Gamma = 10^{-7}$. The eigenvalues approach their common asymptotic limit as

$$|\langle c_i \rangle - 2\mu| = 2\mu \left(\frac{N}{N_E} \right)^{-k_c}, \quad (3)$$

with $k_c = 1/2$ and N_E being slightly dependent on the considered eigenvalue, as illustrated for $\Gamma = 10^{-7}$ and $\Gamma = 2 \times 10^{-8}$ (data scaled by a factor of 5) in Fig. 2(c).

For each cooling rate, we also compute $\langle |\langle c_i \rangle - 2\mu| \rangle$, where $\langle \cdot \rangle$ denotes an average over different realizations and $\langle \langle \cdot \rangle \rangle$ denotes averages over the different eigenvalues. Figure 2(d) shows that this quantity scales as $N^{-1/2}$ for $N > N_E$, with N_E increasing as the cooling rate decreases, as in Fig. 2(d). We remark that N_E can be identified by the

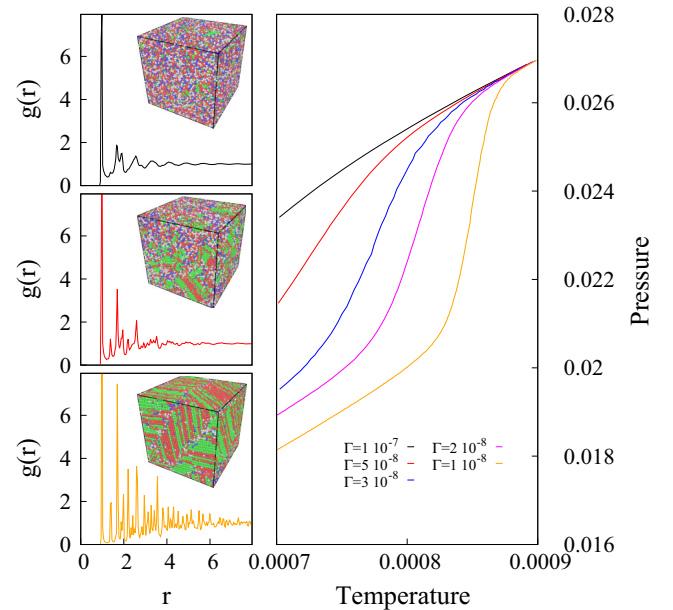


FIG. 1. We illustrate in the right panel the dependence of the pressure on the temperature for different cooling rates. Energy minimization of the $T = 7 \times 10^{-4}$ configuration generates solids solid configurations with different degrees of disorder. The left panels illustrate example radial distribution functions and snapshots of these solids, for $N = 131\,072$. The color of a particle identifies its local crystal structure [20,21]: fcc (green), hpc (red), bcc (blue), icosahedral (yellow), and none (gray). In this work, we investigate the elastic properties of these solids in the linear response regime.

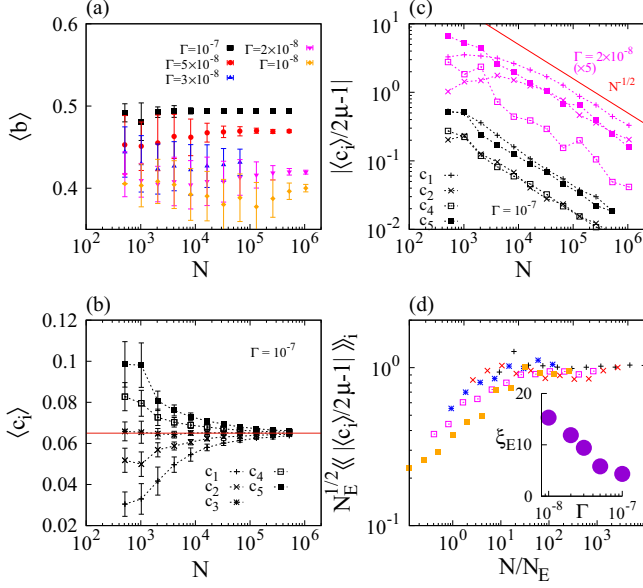


FIG. 2. System size dependence (a) of the largest eigenvalue of the stiffness matrix for different cooling rates and (b) of the other five eigenvalues c_1, \dots, c_5 for $\Gamma = 10^{-7}$. (c) The approach of the average of each $\langle c_i \rangle$ to the common asymptotic value 2μ on increasing the system size for $\Gamma = 10^{-7}$ and $\Gamma = 10^{-8}$. Data are averaged over 50 realizations for each system size and cooling rate. (d) The average of the five eigenvalues $\langle c_i \rangle$ approaches its asymptotic limit as $(N_E/N)^{1/2}$. This allows us to define an elastic length scale $\xi_E = N_E^{1/3}$ which grows as Γ decreases, as illustrated in the inset.

disorder parameter introduced by fluctuating elasticity theory [22–25]. Furthermore, we notice that these findings are in line with previous results on the dependence of the sample-to-sample fluctuations of the elastic constants on the systems size [26–28].

However, these results represent a significant departure from previous findings [6] on the dependence of the stiffness matrix’s eigenvalues on a coarse-grained length scale w . Indeed, this previous work in two spatial dimensions found the largest eigenvalue approaches its asymptotic limit as w^{-2} and the other two approach theirs as $w^{-0.87}$. By associating the exponents with volume and surface effects [6], the scalings should be w^{-3} and w^{-2} in three spatial dimensions, corresponding to $k_b = 1.5$ and $k_c = 1$, in marked contrast to our findings of 0 and 0.5, respectively.

IV. SIZE EFFECTS AS PERTURBATIONS

We rationalize our findings considering that the stress change resulting from an applied deformation is

$$d(\sigma_{\alpha\beta}) = d(\epsilon_{\gamma\delta})c_{\alpha\beta\gamma\delta}(N) = \frac{\rho}{N} \sum_i d(r_{\alpha}f_{\beta})_i, \quad (4)$$

where r_{α} and f_{β} are the α and β components of the distance and the interaction force of the particles involved in bond i , respectively, where a bond corresponds to an interparticle interaction. Since the strain is given, each matrix element $c_{\alpha\beta\gamma\delta}(N)$ is the average of αN numbers. If the contributions $d(r_{\alpha}f_{\beta})_i$ are asymptotically uncorrelated, then by the central

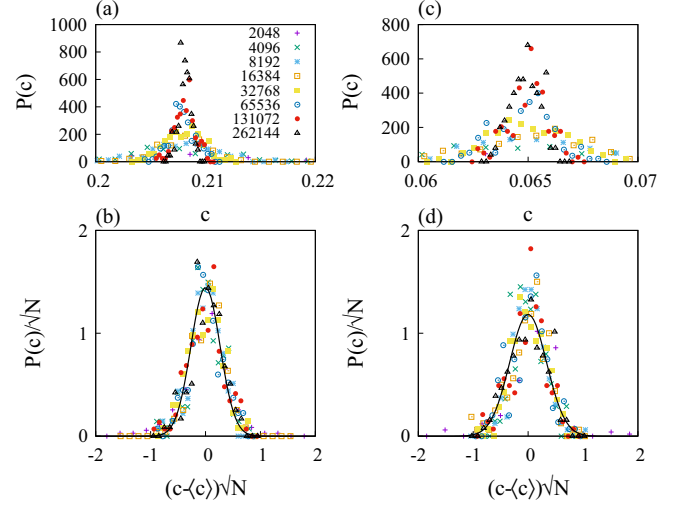


FIG. 3. The distribution of the tensor elements (a) c_{11}, c_{22}, c_{33} and (c) c_{44}, c_{55}, c_{66} for different system sizes at a cooling rate of 10^{-7} . These distributions are respectively collapsed in (b) and (d). The solid lines are Gaussian fits to the $N = 65\,536$ data.

limit theorem each matrix element is Gaussian distributed with average $c_{\alpha\beta\gamma\delta}$, its expected value in the thermodynamic limit, and variance scaling as $N^{-1/2} \propto L^{-d/2}$ in d spatial dimensions. Indeed, we observe in Fig. 3 that the distributions of the matrix elements collapse on a Gaussian curve when appropriately scaled. We remark that these collapses occur only asymptotically, $N > N_E$, implying the existence of short-range spatial correlations between the contributions of the different contacts to the stiffness matrix.

These findings imply that, for $N > N_E$, the stiffness matrix of a given realization is

$$\hat{\mathbf{C}}(N) = \hat{\mathbf{C}}(\infty) + \frac{1}{\sqrt{N}}\hat{\mathbf{R}}, \quad (5)$$

where $\hat{\mathbf{C}}(\infty)$ is as in Eq. (1) and $\hat{\mathbf{R}}$ is a Hermitian random matrix, with some given probability distribution and norm. Finite-size effects, therefore, are equivalent to a random perturbation of the asymptotic stiffness matrix. Matrix perturbation theory [29] then implies that each eigenvalue of $\hat{\mathbf{C}}(N)$ differs from its asymptotic limit by a constant proportional to the spectral norm of the perturbation $N^{-1/2}$, as we have observed.

This theoretical interpretation allows rationalizing the results of Fig. 2, where we investigate how the averages of the sorted eigenvalues of the perturbed matrix approach their asymptotic values. In a given realization, eigenvalue b , which is the largest, equals $b(N) = b_{\infty} + x$, where x is a random number of zero mean and standard deviation $\propto N$. The average over different configurations is therefore $\langle b \rangle(N) = b_{\infty}$: The average has no size dependence, i.e., $k_b = 0$, consistent with our observation in Fig. 1(a). The other five eigenvalues coincide in the thermodynamic limit. At any finite N , noise splits their values, and the eigenvalues equal $c_i = c_{\infty} + x_i$, $i = 1, 5$, where x_i are random variables of zero mean and standard deviation $\propto N^{-1/2}$. Since we sort the eigenvalues, $x_i < x_{i+1}$, we have $|\langle c_i \rangle - c_{\infty}| \propto N^{-k_c}$, with $k_c = 1/2$, for

$i \neq 3$. Conversely, for $i = 3$ we predict $\langle c_i \rangle = c_\infty$. All of these predictions are in agreement with our findings in Fig. 2.

In two dimensions, where the stiffness matrix has three eigenvalues, we predict $k_b = 0$ and $k_c = 1/2$ for $i = 1, 2$. This prediction for k_c is in rough agreement with previous results [6], which reported $2k_c = 0.87$.

V. MECHANICAL AND STRUCTURAL LENGTH SCALES

A. Elastic length scale

The above results imply that the emergence of LIE is characterized by a typical size N_E , with which we associate a length scale $\xi_E := N_E^{1/d}$. For $N > N_E$, the probability distributions of different matrix elements are Gaussian, and Eq. (3) holds. This length scale measures the spatial correlation of different contacts' contributions to the stiffness matrix $d(r_\alpha f_\beta)_i$.

Here, we extract this length scale via the linear regression fits shown in Fig. 2(d). The length scale ξ_E grows as the cooling rate Γ decreases and the system becomes more ordered. It varies from $\xi_E \simeq 4\sigma$ at $\Gamma = 10^{-7}$ to $\xi_E \simeq 15\sigma$ at $\Gamma = 10^{-8}$.

B. Structural length scale

In polycrystalline materials that are an agglomerate of randomly oriented grains, ξ_E is expected to correspond to the typical grain size. In amorphous materials, ξ_E may reflect a structural length scale of difficult definition. Since the correlation between mechanical and geometrical properties of solids is debated [14], it is also possible that ξ_E does not have a structural interpretation.

Here, we investigate the correlation between the elastic and structural properties of our systems by associating with each particle its Steinhardt [30] order parameters, $q_{lm}(i) = \frac{1}{N_b(i)} \sum Y_{lm}(\mathbf{r}_{ij})$, where the sum runs over all N_b neighbors of particle i and $Y_{lm}(\mathbf{r}_{ij}) = Y_{lm}(\theta_{ij}, \psi_{ij})$ are the spherical harmonics. We identify the neighbors through a Voronoi tessellation. The scalar product $s_{ij} = \sum_{m=-6}^6 q_{6m}(i)q_{6m}^*(j)$ measures the correlation between the structures surrounding particles i and j [31]. Hence, the decay of the correlation function

$$S(r) = \frac{\sum_i \sum_j s_{ij} \delta(r - r_{ij})}{\sum_i \sum_j \delta(r - r_{ij})} \quad (6)$$

allows us to estimate a structural correlation length.

We find the correlation function $S(r)$ to decay exponentially, $S(r) = \exp(-r/\xi_S)$, with a characteristic structural length scale ξ_S depending on the cooling rate, as shown in Fig. 4(a). Deviations from the exponential behavior result from finite-size effects. The elastic length scale ξ_E and the structural length scale ξ_S turn out to be proportional, as illustrated in Fig. 4(b). This result demonstrates a close connection between structural and elastic properties, equally valid in our polycrystalline and disordered systems.

C. Stress length scale

Microscopically, ξ_E is the correlation length between the contributions of different interparticle contacts to the stiffness matrix $d(r_\alpha f_\beta)_i$, Eq. (4). One may, therefore, wonder whether the contributions $(r_\alpha f_\beta)_i$ of the contacts to the stress are sim-

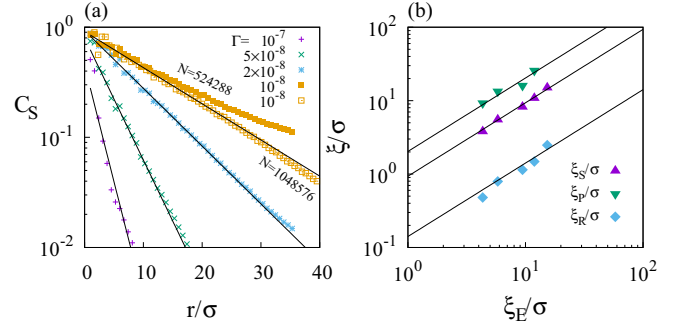


FIG. 4. (a) Structural correlation function, Eq. (6), for different cooling rates and $N = 524288$; for $\Gamma = 10^{-8}$, we also consider a larger N value, as indicated. The exponential decay of the correlation functions defines a structural length scale ξ_S . (b) ξ_S and the length scales ξ_P and ξ_R associated with the pressure and the stress anisotropy, respectively, are proportional to ξ_E .

ilarly correlated. We investigate this issue while focusing on the dependence of the average pressure $\langle P \rangle$ on the system size. Figure 5(a) illustrates that the average pressure exponentially approaches its asymptotic value as N increases. This allows defining a typical size N_P and hence a typical pressure length scale $\xi_P := N_P^{1/d}$, which we show is proportional to ξ_E in Fig. 4(b). We remark here that, for $\Gamma = 10^{-8}$, the pressure dependence on N is too weak to allow for a reliable estimation of ξ_P .

Furthermore, we evaluate the degree of anisotropy of the stress tensor through the parameter $R = \sqrt{2J_2}/P$, where J_2 is the second invariant of the deviatoric stress. Regardless of the cooling rate, $\langle R \rangle$ asymptotically scales as $(N/N_R)^{-1/2}$, as we illustrate in Fig. 5(b). The corresponding length scale $\xi_R := N_R^{1/d}$ is also proportional to ξ_E , as we illustrate in Fig. 4(b).

VI. LOCAL ELASTICITY

We now consider the possibility of extracting the elastic length scale via the direct study of the local elastic properties, rather than resorting to finite-size investigations. To this end, we associate with each particle stress and elasticity tensors. We define the stress tensor of particle i as $\sigma_{\alpha\beta}^{(i)} = \frac{\rho}{2} \sum_j^{(i)} (r_\alpha f_\beta)_j$, where the sum is over all interaction forces

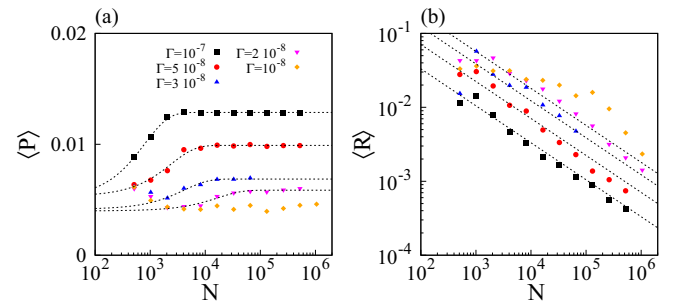


FIG. 5. (a) The average pressure approaches a limiting value as the system size increases. The size dependence is well described by an exponential law, $P = P_0 + \Delta P e^{-N/N_P}$ (lines). (b) The averaged stress anisotropy parameters exponentially scale as $(N/N_R)^{-1/2}$.

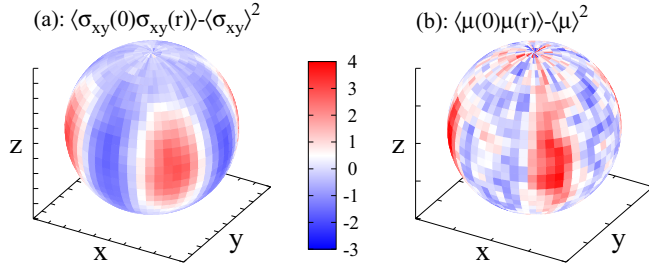


FIG. 6. (a) Spherical map of the correlation function of the particle-level stress, $\langle \sigma_{xy}(0)\sigma_{xy}(r) \rangle - \langle \sigma_{xy} \rangle^2$ [Fig. 6(a)], and of c_{44} , which we will refer to as the local shear modulus μ , $\langle \mu(r)\mu(0) \rangle - \langle \mu \rangle^2$ [Fig. 6(b)], at $r \simeq 1.5$ for an $N = 131\,072$ particle system in a disordered state, as obtained using the fastest of our cooling rates. The standard deviation of the correlations at the considered radial distance is used as a normalization factor. In accordance with previous results [15–18] this investigation evidences Eshelby-like quadrupolar anisotropic correlations both in the stress and in the local shear modulus.

involving particle i . We define a particle-level stiffness tensor $c_{\alpha\beta\gamma\delta}^{(i)}$ as $d\sigma_{\alpha\beta}^{(i)}/d(\epsilon_{\gamma\delta})$. These two definitions and, in particular, the adoption of a uniform strain ensure that the macroscopic stress and stiffness tensors emerge as the average of the local ones.

We illustrate in Fig. 6 spherical maps of the correlations functions of the local shear stress, $\langle \sigma_{xy}(r)\sigma_{xy}(0) \rangle - \langle \sigma_{xy} \rangle^2$ [Fig. 6(a)], and of c_{44} , which we will refer to as the local shear modulus μ , $\langle \mu(r)\mu(0) \rangle - \langle \mu \rangle^2$ [Fig. 6(b)], at $r \simeq 1.5$ for an $N = 131\,072$ particle system in a disordered state, as obtained using the fastest of our cooling rates. The standard deviation of the correlations at the considered radial distance is used as a normalization factor. In accordance with previous results [15–18] this investigation evidences Eshelby-like quadrupolar anisotropic correlations both in the stress and in the local shear modulus.

We investigate the radial dependence of the observed stress correlations through [32] an angle averaged correlation function, $C_{\sigma_{xy}}(r) = -\frac{1}{2\pi} \int_0^\pi d\phi \int_0^{2\pi} d\theta [\langle \sigma_{xy}(r)\sigma_{xy}(0) \rangle - \langle \sigma_{xy} \rangle^2]$. The correlation function $C_\mu(r)$ of the local shear modulus is similarly defined. Figure 7(a) illustrates that $C_{\sigma_{xy}}(r) \propto r^{-3}$, after a transient, regardless of the cooling rate. A similar result holds for the local shear modulus's correlation function, as illustrated in Fig. 7(b). These results confirm the existence of long-range anisotropic correlations [15–18] in the stress and stiffness fields of amorphous materials.

When the correlation functions are plotted versus the radial distance scaled by the elastic length scale, as in Figs. 7(c) and 7(d), data for different cooling rates collapse in the asymptotic regime, within our numerical uncertainty. This result indicates that the correlation functions asymptotically decay as $(r/\xi_e)^{-3}$, demonstrating how the elastic length scale can be evaluated from the analysis of locally defined elastic quantities.

We finally remark that self-averaging, the scaling of the fluctuations of the elastic properties with $N^{-1/2}$ (Fig. 2), holds as these long-range correlations are anisotropic in space. Positive and negative contributions cancel when evaluating the fluctuations via a volume integral of the correlation function.

VII. CONCLUSIONS

Our results establish that the emergence of isotropic linear elasticity is governed by the central limit theorem, whose

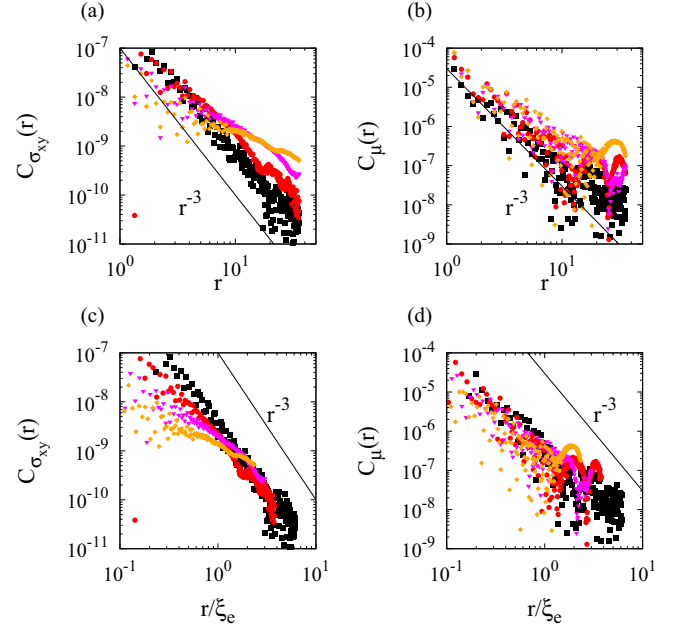


FIG. 7. Correlation function of the particle defined σ_{xy} for different cooling rates, plotted as a function (a) of r and (c) of r/ξ_e . (b) and (d) Analogous results for the correlation function of the particle defined c_4 , respectively. The correlation functions are averaged taking into consideration the quadrupolar symmetry of the fields. Symbols are as in Fig. 5.

predictions are verified in systems larger than a typical elastic length scale. The existence of a finite correlation length in the elastic properties is in general agreement, e.g., with the assumptions of fluctuating elasticity theory [22–24], as well as with the size dependence of the shear modulus reported in previous works [26–28,33]. The degree of disorder does not qualitatively affect this scenario but influences the value of the elastic length scales. Specifically, the elastic length scale grows with the degree of ordering and can be identified with the size of the grain boundaries in polycrystalline materials. We have further demonstrated that the elastic length scale, which we have derived via a finite-size scaling investigation, can alternatively be measured via the study of the spatial correlation of locally defined elastic properties.

The finite-size scaling and real space investigations indicate that the correlation of the elastic properties reflect those of the frozen-in stress. This is a result of practical significance, as correlations in the stress are easier to investigate than correlations in the local elastic constants.

We suspect that the structural correlation function we have introduced may be inappropriate in the presence of polydispersity or nonradially symmetric interaction potentials. In these cases it is not apparent which structural correlation function relates to the elastic response. Possibly, in these cases structural correlations could be more meaningfully indirectly evaluated by studying the correlation of the elastic properties. This appears to be a promising direction to extract a static length scale in disordered materials whose relevance to, e.g., the glass transition problem [34] or plastic response [3] needs to be systematically explored.

In this regard, it is interesting to contrast our results with size-scaling studies of the fluctuations of the shear modulus in systems whose crystallization is severely inhibited. These studies considered systems first thermalized at a parent temperature T_p and then brought to an energy minimal configuration. The parent temperature, therefore, qualitatively plays the role of our cooling rate. While we have observed that the elastic length scale grows as a system is better annealed, correlated to the size of the grain boundaries, these previous studies have conversely found it to decrease [25,35]. Recent results [25,36,37] have also shown that, in attractive systems, the elastic length scale is affected by the range of the attractive

interaction. Hence, depending on the features of the underlying energy landscape, annealing might increase or decrease the elastic length scale above which isotropic linear elasticity sets in.

ACKNOWLEDGMENTS

We acknowledge support from the Singapore Ministry of Education through the Academic Research Fund Tier 1 (2019-T1-001-03) and are grateful to the National Supercomputing Centre (NSCC) of Singapore for providing the computational resources.

-
- [1] R. Mullen, R. Ballarini, Y. Yin, and A. Heuer, Monte Carlo simulations of effective elastic constants of polycrystalline thin films, *Acta Mater.* **45**, 2247 (1997).
- [2] J. P. Wittmer, A. Tanguy, J.-L. Barrat, and L. Lewis, Vibrations of amorphous, nanometric structures: When does continuum theory apply? *Europhys. Lett.* **57**, 423 (2002).
- [3] J. P. Sethna, M. K. Bierbaum, K. A. Dahmen, C. P. Goodrich, J. R. Greer, L. X. Hayden, J. P. Kent-Dobias, E. D. Lee, D. B. Liarte, X. Ni, K. N. Quinn, A. Raju, D. Z. Rocklin, A. Shekhawat, and S. Zapperi, Deformation of crystals: Connections with statistical physics, *Annu. Rev. Mater. Res.* **47**, 217 (2017).
- [4] A. Tanguy, J. P. Wittmer, F. Leonforte, and J.-L. Barrat, Continuum limit of amorphous elastic bodies: A finite-size study of low-frequency harmonic vibrations, *Phys. Rev. B* **66**, 174205 (2002).
- [5] F. Leonforte, R. Boissière, A. Tanguy, J. P. Wittmer, and J.-L. Barrat, Continuum limit of amorphous elastic bodies. III. Three-dimensional systems, *Phys. Rev. B* **72**, 224206 (2005).
- [6] M. Tsamados, A. Tanguy, C. Goldenberg, and J. L. Barrat, Local elasticity map and plasticity in a model Lennard-Jones glass, *Phys. Rev. E* **80**, 026112 (2009).
- [7] A. Cakir and M. Pica Ciamarra, Emergence of linear elasticity from the atomistic description of matter, *J. Chem. Phys.* **145**, 054507 (2016).
- [8] H. Mizuno, S. Mossa, and J.-L. Barrat, Measuring spatial distribution of the local elastic modulus in glasses, *Phys. Rev. E* **87**, 042306 (2013).
- [9] W. Voigt, Ueber die Beziehung zwischen den beiden Elasticitätsconstanten isotroper Körper, *Ann. Phys. (Berlin, Ger.)* **274**, 573 (1889).
- [10] A. Reuss, Berechnung der fließgrenze von mischkristallen auf grund der plastizitätsbedingung für einkristalle, *Z. Angew. Math. Mech.* **9**, 49 (1929).
- [11] G. Mavko, T. Mukerji, and J. Dvorkin, *The Rock Physics Handbook* (Cambridge University Press, Cambridge, 2009).
- [12] M. Avellaneda, A. V. Cherkaevj, L. V. Gibiansky, G. W. Milton, and M. Rudelsont, A complete characterization of the possible bulk and shear moduli of planar polycrystals, *J. Mech. Phys. Solids* **44**, 1179 (1996).
- [13] P. M. Chaikin and T. C. Lubensky, *Principles of Condensed Matter Physics* (Cambridge University Press, Cambridge, 2010).
- [14] C. P. Goodrich, A. J. Liu, and S. R. Nagel, Solids between the mechanical extremes of order and disorder, *Nat. Phys.* **10**, 578 (2014).
- [15] A. Lemaître, Structural Relaxation Is a Scale-Free Process, *Phys. Rev. Lett.* **113**, 245702 (2014).
- [16] B. Wu, T. Iwashita, and T. Egami, Anisotropic stress correlations in two-dimensional liquids, *Phys. Rev. E* **91**, 032301 (2015).
- [17] A. Lemaître, Tensorial analysis of Eshelby stresses in 3D supercooled liquids, *J. Chem. Phys.* **143**, 164515 (2015).
- [18] A. Lemaître, Stress correlations in glasses, *J. Chem. Phys.* **149**, 104107 (2018).
- [19] J. C. Pàmies, A. Cacciuto, and D. Frenkel, Phase diagram of Hertzian spheres, *J. Chem. Phys.* **131**, 044514 (2009).
- [20] G. J. Ackland and A. P. Jones, Applications of local crystal structure measures in experiment and simulation, *Phys. Rev. B* **73**, 054104 (2006).
- [21] A. Stukowski, Visualization and analysis of atomistic simulation data with OVITO—The Open Visualization Tool, *Modell. Simul. Mater. Sci. Eng.* **18**, 015012 (2010).
- [22] W. Schirmacher, G. Ruocco, and T. Scopigno, Acoustic Attenuation in Glasses and Its Relation with the Boson Peak, *Phys. Rev. Lett.* **98**, 025501 (2007).
- [23] W. Schirmacher, Thermal conductivity of glassy materials and the “boson peak,” *Europhys. Lett.* **73**, 892 (2006).
- [24] A. Marruzzo, W. Schirmacher, A. Fratallocchi, and G. Ruocco, Heterogeneous shear elasticity of glasses: The origin of the boson peak, *Sci. Rep.* **3**, 1407 (2013).
- [25] S. Mahajan, K. González-López, E. Lerner, and M. Pica Ciamarra (unpublished).
- [26] H. Mizuno, S. Mossa, and J.-L. Barrat, Relation of vibrational excitations and thermal conductivity to elastic heterogeneities in disordered solids, *Phys. Rev. B* **94**, 144303 (2016).
- [27] H. Mizuno, K. Saitoh, and L. E. Silbert, Elastic moduli and vibrational modes in jammed particulate packings, *Phys. Rev. E* **93**, 062905 (2016).
- [28] G. Kapteijns, D. Richard, E. Bouchbinder, and E. Lerner, Elastic moduli fluctuations predict wave attenuation rates in glasses, *J. Chem. Phys.* **154**, 081101 (2021).
- [29] G. W. Stewart and J.-G. Sun, *Matrix Perturbation Theory* (Academic, 1990), p. 365.
- [30] P. J. Steinhardt, D. R. Nelson, and M. Ronchetti, Bond-orientational order in liquids and glasses, *Phys. Rev. B* **28**, 784 (1983).

- [31] W. Lechner and C. Dellago, Accurate determination of crystal structures based on averaged local bond order parameters, *J. Chem. Phys.* **129**, 114707 (2008).
- [32] H. Tong, S. Sengupta, and H. Tanaka, Emergent solidity of amorphous materials as a consequence of mechanical self-organisation, *Nat. Commun.* **11**, 4863 (2020).
- [33] E. Lerner, Mechanical properties of simple computer glasses, *J. Non-Cryst. Solids* **522**, 119570 (2019).
- [34] S. Karmakar, C. Dasgupta, and S. Sastry, Growing length and time scales in glass-forming liquids, *Proc. Natl. Acad. Sci. USA* **106**, 3675 (2008).
- [35] C. Rainone, E. Bouchbinder, and E. Lerner, Pinching a glass reveals key properties of its soft spots, *Proc. Natl. Acad. Sci. USA* **117**, 5228 (2020).
- [36] K. González-López, M. Shivam, Y. Zheng, M. P. Ciamarra, and E. Lerner, Mechanical disorder of sticky-sphere glasses. I. Effect of attractive interactions, *Phys. Rev. E* **103**, 022605 (2021).
- [37] K. González-López, M. Shivam, Y. Zheng, M. P. Ciamarra, and E. Lerner, Mechanical disorder of sticky-sphere glasses. II. Thermomechanical inannealability, *Phys. Rev. E* **103**, 022606 (2021).